Hydrodynamic characteristics of the modified V-shaped Semi-floating offshore wind turbine with heave plates

IOP Conf. Series: Journal of Physics: Conf. Series **1356** (2019) 012017 doi:10.1088/1742-6596/1356/1/012017

Hydrodynamic characteristics of the modified V-shaped Semi-floating offshore wind turbine with heave plates

Wei Shi[1], Lixian Zhang[1], Jikun You[2], Madjid Karimirad[3] and Constantine Michailides[4]

[1]Deepwater Engineering Research Center, State Key Laboratory of Coast and Offshore Engineering, Dalian University of Technology, Dalian, Liaoning, China,

[2] Connect Lng AS, Oslo, Norway

[3]Marine and Coastal Engineering, School of Natural and Built Environment, Queen's University Belfast, Belfast, UK

[4]Department of Civil Engineering and Geomatics, Cyprus University of Technology, Limassol, Cyprus

Email: weishi@dlut.edu.cn

Abstract. In recent years, there is a great need to develop offshore wind energy on a global scale due to the greenhouse effect and energy crisis. Great efforts have been devoted to developing a reliable floating offshore wind energy technology to take advantage of the large amount of wind energy resources that exist in deep water. In this paper, a novel concept of a floating offshore wind turbine (FOWT), namely, the modified V-shaped semi-floating with heave plate, is proposed, and its hydrodynamic characteristics are studied. A numerical model based on ANSYS/AQWA is used to investigate the dynamic motion, response characteristics and mooring performance of the new concept. Moreover, the response amplitude operators (RAOs) of the different response quantities are also elaborated. A comparative study of the dynamic response of the different response quantities of the modified V-shape and original V-shaped semi-floating is carried out for operational environmental conditions. It is found that the modified V-shape semi-floating shows relatively better performance in platform motion and mooring line response.

1. Introduction

Renewable energy has received keen interest in a sustainable future given the fact it plays an important role for reducing greenhouse gas emissions, and thus in mitigating climate change. Moreover, the dramatic increase in energy demand leads to a higher renewable energy need. Offshore wind energy is recognized as one of the world's fastest-growing renewable energy resources. There is a large ambition for offshore wind energy in the next ten years. According to a new analysis from the International Renewable Energy Agency (IRENA) [1], offshore wind power has the potential to grow from 12 GW in 2015, to 100 GW in 2030, driven by technology advancements and further cost declines.

In shallow waters and intermediate water depth (less than 60 m), offshore wind turbines are usually installed on a fixed substructure. Moving towards deep waters provides better wind condition with less turbulence and reduces the area limitation, noise and visual impact problems. Floating wind turbine seems more economically feasible for deep-water zones. A disadvantage of floating wind turbines is their increased dynamic motions; hence, the importance of research on its dynamic behaviour should be addressed. Dated back to the year of 1972, Heronemus [2] proposed a concept of a floating platform on which a number of wind turbines are mounted. Since then, various types of

floating offshore wind turbines (FOWTs) have been proposed. Based on the fundamental principles adopted to achieve static stability, a floating platform can be classified into three primary concepts [3]: a semisubmersible, a spar buoy and a tension-leg platform (TLP). Among the different concepts of FOWTs, the semisubmersible platform is considered to be a very economical construction that relies on large water plane, as well as ballasting, to maintain stability. The world first floating wind turbine, a 2.3 MW spar-type Hywind deployed about 10 km off the island of Karmøy in Norway, has successfully operated since 2009 [4]. Equinor (Previously named Statoil) developed the first floating wind farm, Hywind Scotland, with full grid connection in 2017 [5]. Spar buoy platform with simple structure shows good stability and less motion. However, it needs a large water depth and large installation cost. TLP platform has good motion response but has a high cost of tendon lines and installation. Compared with the other FOWT concepts, the main advantages of semi-floating platforms include, but are not limited to: a) it can be fully constructed onshore where the quality is easily assured and towed to specified offshore site, eliminating the need for expensive construction barges and ship crane; b) the catenary mooring system that is usually employed in semisubmersible platform design leads to lower installed mooring cost.

Bulder [6] investigated the different concepts of the semisubmersible platform, circular, triangular, and quadrilateral floating foundation, and noted that the triangular floating foundation is feasible in terms of stability as well as low construction cost. Since then, most concept designs of semisubmersible FOWTs employ the triple-floater foundation, such as the OC4-DeepCwind FOWT [7], WindFloat [8], Braceless [9], V-shaped semi-floating FOWT [10-14]. Robertson and Jonkman [15] conducted a comprehensive dynamic-response analysis of six offshore floating wind turbine concepts, represented by TLP, Barge, OC4-DeepCwind semisubmersible FOWT and Spar buoy, together with the NREL 5WM baseline wind turbine. The dynamic performance of these models was simulated via the FAST-WAMIT coupled tool. The results show that the loads between TLP, Spar and OC4-DeepCwind semisubmersible FOWT are similar. Aubault [16] discusses the preliminary structural assessment of FOWTs focusing on the methodology designed to estimate the strength and fatigue of the WindFloat's novel structural components. This work concluded that it is essential to incorporate the effect of aerodynamics in the detailed structural analysis. Xu and Gao[9] studied the response of the Braceless FOWT and its mooring system in shallow water depths. Three mooring design concepts in 200 m, 100 m and 50 m water depths were proposed for the 5 MW CSC FOWT. The research showed that the contribution of hydrodynamic load from different frequency become increasingly significant as water depth decreases. The quadratic transfer function (QTF) method is recommended to accurately obtain the low-frequency response.

Several research studies of the V-shaped semi FOWT have been conducted by Karimirad and Michailides [10-14]. The Stochastic dynamic motion responses and generated power of a semisubmersible floating wind turbine for different water depths of 100 m and 200 m [13] were examined for selected environmental conditions by using fully coupled method. The results showed that the generated power and behavior of the floating wind turbine is not greatly dependent on water depths if a proper mooring system is applied. The developed and applied process for the appropriate design of the mooring lines is generic and can be applied for different semisubmersible wind turbine concepts or catenary moored floating wind turbines. The dynamic response of the V-shaped semi FOWT under different fault condition was carried out with the use of coupled analysis tool Simo-Riflex-AeroDyn [14]. The research indicates that the shutdown case seems to affect the dynamic response of the V-shaped semi FOWT, mostly among fault conditions.

To minimize the heave and pitch motion, heave plates are often attached to semisubmersible platform's base, such as OC4-DeepCwind, WindFloat and OO-Star wind floater [17]. The hydrodynamic effects of the heave plate design for semisubmersible offshore wind turbine has been discussed by Lopez-Pavon and Souto-Iglesias [18]. Jiang and Hu [19] propose a novel semisubmersible platform based on WindFloat, referred to as HexaSemi. Compared with WindFloat, the new damping plate has a single triangle shape with a moonpool. The performance of HexSemi platform is better than WindFloat under extreme wind and wave load conditions in terms of heave

and pitch motion as well as mooring line performance.

In this paper, a novel concept of the semisubmersible FOWT, the modified V-shape semi-floating with a heave plate, is introduced to minimize the heave and pitch motion, as shown in Figure 1. A deep-water offshore site with a depth of 200 m is selected. The work herein presents a comprehensive dynamic-response analysis of V-shaped semi-floating and modified the V-shaped semi-floating under several of wave-wind induced load cases. The performance of both FOWTs is evaluated via ANSYS/AQWA. It is found that the modified V-shape semi-floating shows relative better performance in platform motion and mooring line response compared to the design of the V-semi-floating without the use of heave plates.

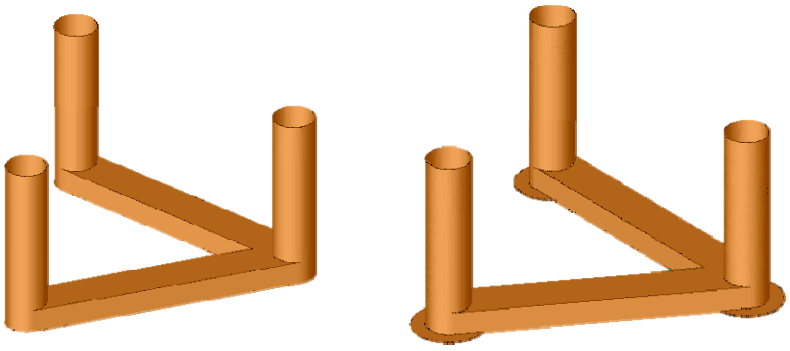

Figure 1. Concept of V-shaped semi-floating and modified V-shaped semi-floating

2. Characteristics of the V-shaped semi FOWT and the modified V-shaped semi FOWT

The wind turbine used in this paper is developed by NREL; it is a conventional variable speed, upwind, collective pitch horizontal axis wind turbine. The V-shaped semi-floating platform used in this paper consists of three columns (one center column and two side columns) and two pontoons connecting the side columns to center column. Compared to V-shaped semi-floating, the modified V-shaped semi-floating has a heave plate below the center column and side columns with a diameter of 15 m. The detailed parameters of the two FOWT systems are listed in Table 1.

Table 1. V-shaped semi and modified V-shaped semi FOWT system parameters

Variable	V-shaped semi-floating	modified V-shaped semi-floating
Distance between columns (m)	60	60
Center column height (m)	38	38
Side column height (m)	48	48
Draft (m)	28	28
Pontoon dimensions: width*height (m*m)	9*5	9*5
Angle between pontoons	60	60
Diameter of columns (m)	9	9
Heave plate diameter (m)	none	15
Floater steel mass (kg)	1.630E+6	1.645E+6
Water ballast (kg)	7.873E+6	7.873E+6
Total mass (kg)	1.0263E+7	1.033E+7
Submerged volume (m^3)	10013	10078
COG(x, y, z) (m)	(-30.6,0,-16.0)	(-30.7,0,-16.2)
COB(x, y, z) (m)	(-30.6,0,-19.4)	(-30.7,0,-19.45)
Mass Moment of Inertia I_{xx} ($kg*m^2$)	1.29E+10	1.33E+10
Mass Moment of Inertia I_{yy} ($kg*m^2$)	2.18E+10	2.20E+10

Mass Moment of Inertia I_{zz} (kg*m^2)	1.79E+10	1.80E+10

The V-shaped semi FOWT and the modified V-shaped semi FOWT are connected to the seabed with three single mooring lines as shown in Figure 2. The clump mass is positioned 82 m from the fairlead of each mooring line. The location of fairlead and anchor points is shown in Table 2, and the relevant characteristics of the mooring line are shown in Table 3.

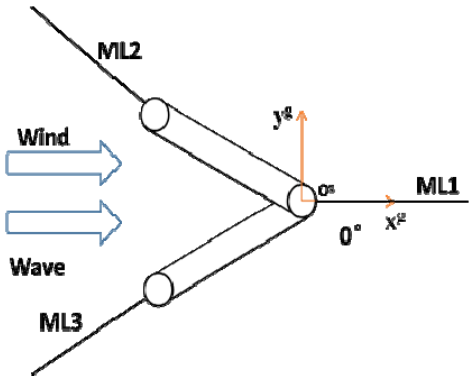

Figure 2. Configuration of the mooring systems of the two platforms

Table 2. Coordinates of fairlead and anchor points of the three mooring lines

Fairlead for line 1 (x, y, z) (m)	(4.5,0,-18)
Anchor point for line 1 (x, y, z) (m)	(650,0,-200)
Fairlead for line 2 (x, y, z) (m)	(-55.8,32.3,-18)
Anchor point for line 2 (x, y, z) (m)	(-618.7,357,-200)
Fairlead for line 3 (x, y, z) (m)	(-55.8,-32.3,-18)
Anchor point for line 3 (x, y, z) (m)	(-618.7,-357,-200)

Table 3. Mooring line characteristics

Variables	Value
Length of each line (m)	700
Mass per meter (kg/m)	117
Equivalent Axial stiffness (N)	3.0E+9
Diameter (m)	0.138
Drag coefficient	1.2
Clump mass (kg)	37000
Clump volume (m^3)	4.4

3. Theory Background

3.1 Equation of motion

The large volume body is represented by a six degree of freedom (6-DOF) rigid body. The load model for the body accounts for the wind and wave loads. The wind acted on the structure and current forces are based on a set of direction-dependent coefficients for each of the DOF. Linear and quadratic forces could also be included. In this paper, the wind and wave loads are considered, and the structural viscous damping is not included. The equation of motion under wind-wave loads in time domain analysis is calculated in ANSYS/AQWA; for rigid body motion of degree of freedom, *j*, it can be expressed as:

$$\sum_{i=1}^{6}\left(\left(M_{ij}+A_{ij}\right)\ddot{x}_j(t)+\int_{-\infty}^{t}\dot{x}_j(\tau)K_{ij}\left(t-\tau\right)d\tau+C_{ij}x(t)\right)=F_{wave,j}\left(t\right)+F_{moor,j}\left(t\right)+F_{wind,j}\left(t\right) \quad (1)$$

where M_{ij} is the mass coefficient, A_{ij} is the added mass coefficient calculated by AWQA-LINE, $K_{ij}(t-\tau)$ is the retardation function which represents the fluid memory effect, C_{ij} is the restoring coefficient calculated by AWQA-LINE, $\ddot{x}$, $\dot{x}$ and x are the acceleration, velocity, and displacement of the platform, $F_{wave,j}(t)$ is the wave exciting force, $F_{wind,j}(t)$ is the aerodynamic force that acts on the rotor and $F_{moor,j}(t)$ is the restoring force that results from mooring lines, j is the DOF in surge, sway, heave, roll, pitch and yaw direction.

3.2 Wind load

A structure under wind flow will experience static and dynamic wind loads. The wind loads acting on the tower and nacelle are mainly drag force. However, the wind loads acting on turbine blades have both lift and drag forces, which can be calculated from blade element momentum (BEM), generalized dynamic wake (GDW) or computational fluid dynamics (CFD). In this paper, the wind load is simplified as a thrust force based on force-wind speed curve of NREL 5 MW baseline wind turbine. The force-speed curve of NREL 5 MW baseline wind turbine is shown in Figure 3.

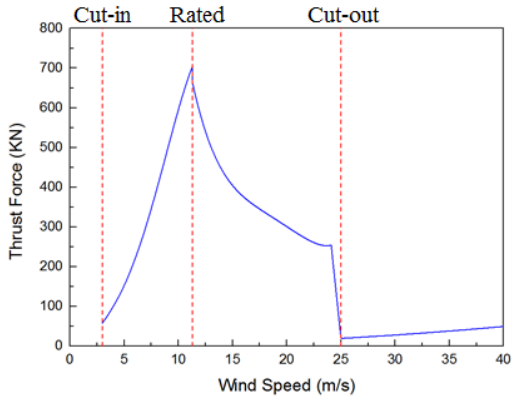

Figure 3. Force-speed curve of NREL 5WM baseline wind turbine

3.3 Hydrodynamic load

The V-shaped semi-floating and the modified V-shaped semi-floating are modelled using boundary element (Figure 4), and the potential flow theory is adapted to calculate the first order hydrodynamic load. The assumption is made that the fluid is irrotational, inviscid and incompressible. In addition, the fluid needs to satisfy the Laplace's equation:

$$\nabla^2\phi^{(1)}=\frac{\partial^2\phi}{\partial x^2}+\frac{\partial^2\phi}{\partial y^2}+\frac{\partial^2\phi}{\partial z^2}=0 \quad (2)$$

where $\phi^{(1)}$ is the first order total velocity potential function involving the incident potential $\phi_i^{(1)}$, diffraction potential $\phi_d^{(1)}$, and radiation potential $\phi_r^{(1)}$. To solve the potential function $\phi^{(1)}$, some boundary conditions are applied as shown below:

$$\frac{\partial\phi}{\partial z}=0, z=-h \quad (3)$$

$$\frac{\partial^2\phi}{\partial t^2}+g\frac{\partial\phi}{\partial z}=0, z=0 \quad (4)$$

$$\frac{\partial\phi}{\partial n}=\sum_{i=1}^{n}v_i f_i\left(x,y,z\right) \quad (5)$$

$$\lim_{R\to\infty}\phi=0 \quad (6)$$

Once $\phi^{(1)}$ is solved, the exciting wave forces and moment can be obtained by integration over the wetted body surface.

$$F_{EXj}^{(1)} = \mathrm{Re}\left\{-\rho A e^{iwt}\iint_S n_j\left(\phi_i+\phi_d\right)dS\right\}, j=1,2,3 \tag{7}$$

$$M_{EXj}^{(1)} = \mathrm{Re}\left\{-\rho A e^{iwt}\iint_S \left(r\times n\right)_j\left(\phi_i+\phi_d\right)dS\right\}, j=4,5,6 \tag{8}$$

where: S express the wetted surface; A is the wave amplitude, j is the degree of freedom (DoF) including surge, sway, heave, roll, pitch and yaw.

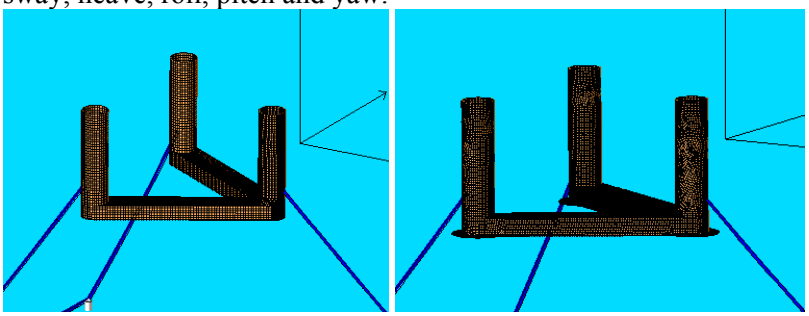

Figure 4. Numerical model of two platforms

3.4 Mooring system

The mooring line force is calculated by employing the lumped mass method in this paper. The mooring line is discretized into a number of finite elements where the mass of each element is concentrated into a corresponding node. The equation of motion of this cable element is:

$$\begin{aligned}&\frac{\partial\vec{T}}{\partial s_e}+\frac{\partial\vec{V}}{\partial s_e}+\vec{w}+\vec{F}_h = m\frac{\partial^2\vec{R}}{\partial t^2}\\&\frac{\partial\vec{M}}{\partial s_e}+\frac{\partial\vec{R}}{\partial s_e}\times\vec{V} = -\vec{q}\end{aligned} \tag{9}$$

where: m is the structural mass per unit length, $\vec{q}$ is the distributed moment loading per unit length, $\vec{R}$ is the position vector of the first node of the cable element, ΔS_e and D_e are the length and diameter of the element, respectively, $\vec{w}$ and F_h are the element weight and external hydrodynamic loading vectors per unit length, respectively, $\vec{T}$ is the tension force vector at the first node of the element, $\vec{M}$ is the bending moment vector at the first node of the element, and $\vec{V}$ is the shear force vector at the first node of the element.

3.5 Heave plate model

The heave plate in modified V-shaped semi-floating is modelled as panel elements. To accurately simulate the fluid pressure on the heave plate, the heave plate is simulated with a very small thickness equal to 0.01 m. Viscous damping equal to 8% of the critical damping in heave motion is added to simulate the damping effect of the heave plate. The viscous damping is calculated from Eq. 10.

$$\begin{aligned}&B_{critical} = 2\sqrt{\left(M+\Delta M\right)K_{stillwater}}\\&B_{vis} = \alpha B_{critical}\end{aligned} \tag{10}$$

where: $B_{critical}$ is the critical damping, and α is the damping ratio.

4 Examined load cases and wave-wind induced dynamics Analysis

4.1 Examined load case

To estimate the dynamic response of the V-shaped semi-floating and modified V-shaped semi-floating in different wave and wind environmental conditions, the hydrodynamic analysis tool-ANSYS/AQWA is used. The examined load conditions representing a high range of possible operational condition according to the relevant sea states in the North Sea, Norway, is applied. The examined mean wind speeds at the hub height, U_w, are presented in Table 4. H_s is the significant wave height and T_p is the wave peak period of the JONSWAP spectrum with 3.3 of the peakedness factor that is used to simulate irregular waves. Wind and wave are both considered aligned with the x-axis.

Table 4. Load cases

Load cases	U_w (m/s)	H_s (m)	T_p (s)	Notes
LC1 (wave-only case)		3.0	10.0	Irregular wave
LC2 (wind+wave)	11.4	5.0	12.0	Constant wind, Irregular wave
LC3 (wind+wave)	17.0	5.0	12.0	Constant wind, Irregular wave
LC4 (wind+wave)	49.0	14.1	13.3	Constant wind, Irregular wave

4.2 Mooring line force-displacement relationships

To investigate the mooring system performance of the V-shaped semi-floating and the modified V-shaped semi-floating, the mooring line force-displacement relationships are calculated by ANSYS/AQWA-Librium. Because the relationships show similar trends, only the force-displacement relationships for V-shaped semi-floating is displayed in Figure 5.

When the platform has a surge displacement, the mooring restoring load exerting on the platform increases rapidly in the V-shaped semi-floating as shown in Figure 5. Due to the asymmetrical characteristic in the pitch direction, the pitch-pitch stiffness of the V-shaped semi-floating is not symmetry with respect to positive and negative pitch displacements. In addition, due to its asymmetrical nature of the V-shaped semi-floating, the heave and roll displacement can lead to pitch restoration, indicating a motion coupling between those modes.

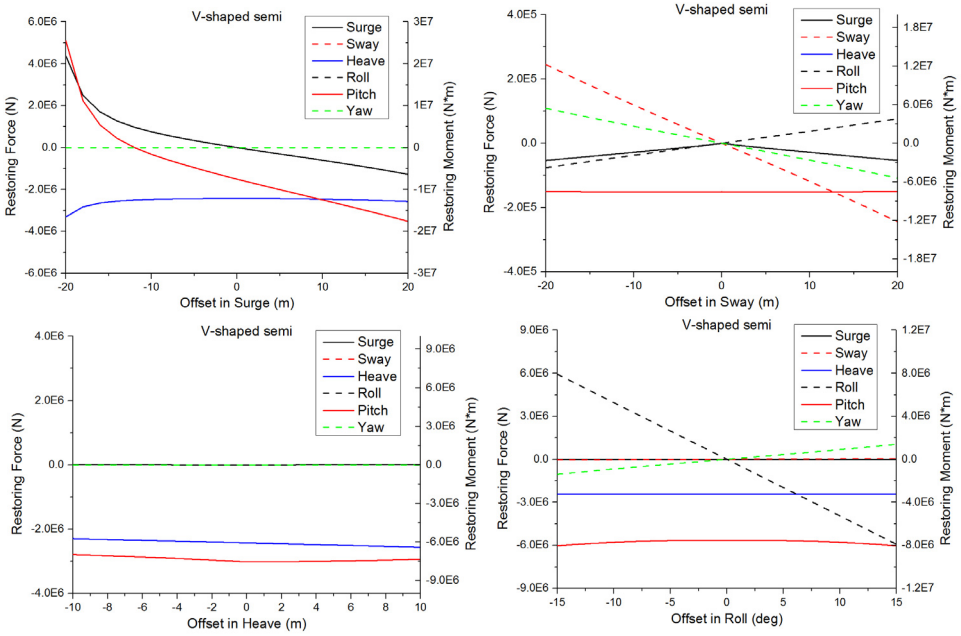

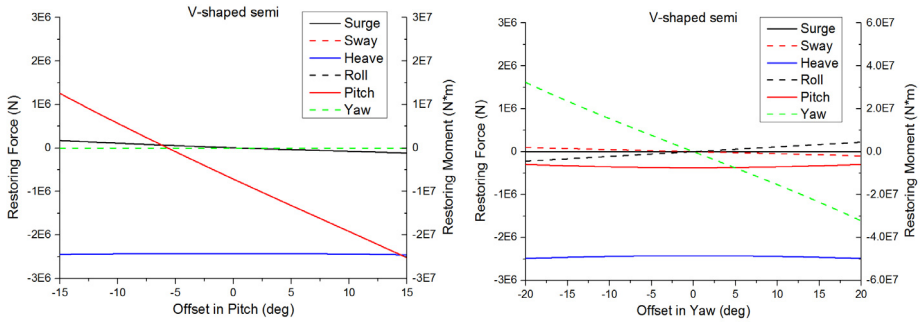

Figure 5. Load-displacement relationships for the V-shaped semi-floating in six DOFs

4.3 Simulation and Results

4.3.1 Response Amplitude Operator of the platforms. Figures 6 presents the predicted RAOs for V-shaped semi-floating and modified V-shaped semi-floating over the wave frequency for the heave and pitch. It can be seen that for heave DOF, there are no significant changes into the response between two platforms only a small different near 0.27 rad/s which is corresponding to pitch frequency. This is due to the motion coupling effect betweem the heave and pitch motion of these two semi-floatings. However, the obtained responses in pitch for modified V-shaped semi-floating have a large reduction near pitch frequency compared with V-shaped semi-floati

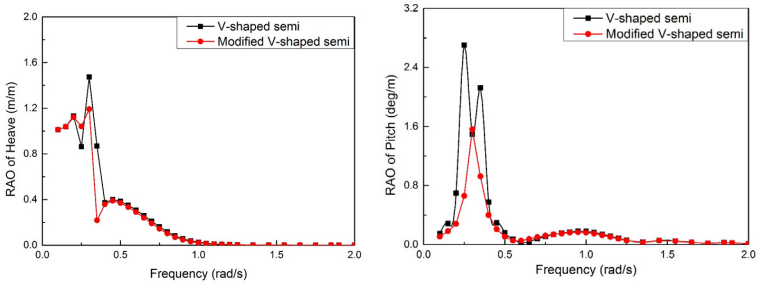

Figure 6. Platform motion RAOs of the platforms

4.3.2 Response of platform motions. The aligned wave-wind condition with a wave heading of 0° was considered for all load cases. Thus, only surge, heave, and pitch floater motions are discussed as an example in this paper. The statistical characteristics of motion under different load cases of two platforms are summarized in Table 5, Table 6 and Table 7, including the mean, maximum, minimum, and standard deviation (STD).

Table 5. Statistical characteristics of surge motion under four load cases

Load cases	Item	Mean (m)	Max (m)	Min (m)	STD (m)
LC1	V-shaped semi-floating	-10.58	-9.68	-11.38	0.26
	Modified V-shaped semi-floating	-10.67	-9.72	-11.46	0.26
LC2	V-shaped semi-floating	1.75	4.28	-0.57	0.74
	Modified V-shaped semi-floating	1.62	4.27	-0.82	0.77
LC3	V-shaped semi-floating	-4.12	-1.54	-6.25	0.72
	Modified V-shaped semi-floating	-4.22	-1.65	-6.36	0.71
LC4	V-shaped semi-floating	-8.15	6.84	-20.65	4.32
	Modified V-shaped semi-floating	-8.52	5.98	-21.84	4.19

Table 6. Statistical characteristics of heave motion under four load cases

Load cases	Item	Mean (m)	Max (m)	Min (m)	STD (m)

LC1	V-shaped semi-floating	-0.18	0.57	-1.02	0.23
	Modified V-shaped semi-floating	0.17	0.94	-0.53	0.18
LC2	V-shaped semi-floating	-2.89	-1.27	-4.28	0.47
	Modified V-shaped semi-floating	-2.57	-1.34	-3.92	0.41
LC3	V-shaped semi-floating	-1.60	-0.17	-3.12	0.48
	Modified V-shaped semi-floating	-1.27	-0.08	-2.64	0.41
LC4	V-shaped semi-floating	-0.62	4.91	-6.18	1.66
	Modified V-shaped semi-floating	-0.26	3.72	-5.16	1.40

Table 7. Statistical characteristics of pitch motion under four load cases

Load cases	Item	Mean (deg)	Max (deg)	Min (deg)	STD (deg)
LC1	V-shaped semi-floating	0.32	0.88	-0.31	0.18
	Modified V-shaped semi-floating	-0.37	0.01	-0.85	0.10
LC2	V-shaped semi-floating	4.79	5.79	3.42	0.33
	Modified V-shaped semi-floating	4.14	4.66	3.38	0.18
LC3	V-shaped semi-floating	2.66	4.03	1.46	0.35
	Modified V-shaped semi-floating	1.99	2.53	1.32	0.18
LC4	V-shaped semi-floating	0.93	7.47	-5.77	2.20
	Modified V-shaped semi-floating	0.18	3.69	-3.50	1.00

Overall, the differences in the motion amplitudes are significant, especially for the heave and pitch motion. Our research found a strong coupling effect between the heave and pitch motion in the modified V-shaped semi-floating. The data indicate that the pitch motion in the modified V-shaped semi-floating has a smaller motion amplitude and standard deviation than those of the V-shaped semi-floating. It is shown that the heave performance of the modified V-shaped semi-floating is slightly better than the V-shaped semi-floating under different load cases.

To investigate the platform from the perspectives of frequency and energy-absorption, we calculate the motion spectra of the platform. The motion spectra of the platform under LC 1 is shown in Figure 7. The research indicates the spectra of the motion responses consist of two parts. The low-frequency part is related with the resonance of the motions while the higher frequency part is related with wave-induced motions; as it is clear in Figure 7, the spectra of lower frequency part in the modified V-shaped semi-floating near pitch natural frequency is lower than that of the V-shaped semi-floating. A possible reason is that the damping plate mounted below V-shaped semi-floating absorbed most of the energy.

The motion spectra of the platform under LC 4 in extreme sea states is shown in Figure 8. Similar as in LC1, significant reduction of the motion responses are found for both heave and pitch motion near pitch natural frequency. But motion reductions near wave frequency are limited.

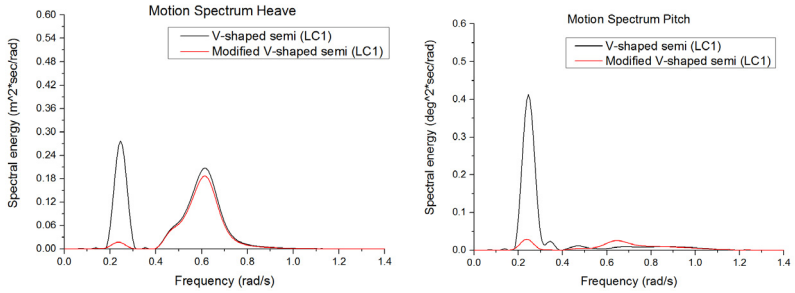

Figure 7. Motion spectra under LC1

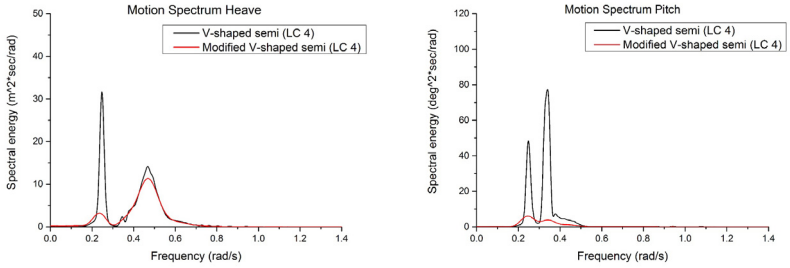

Figure 8. Motion spectra under LC4

4.3.3 Response of mooring system. It is very important to output the values of mooring line tensions under extreme wind-wave induced conditions because the mooring line tension is directly related to the survival capability of the platform. Therefore, only the mooring line tensions between the two platforms under extreme wind and wave load conditions are shown in Figure 7. The statistical characteristics of mooring line force under different LC 4 of two platforms are summarized in Table 8, including the mean, maximum, minimum, and standard deviation.

Table 8. Statistical characteristics of mooring lines force under LC 4

Mooring line	Item	Mean (kN)	Max (kN)	Min (kN)	STD (kN)
ML1	V-shaped semi-floating	1235.5	2088.1	706.8	185.9
	Modified V-shaped semi-floating	1244.8	1998.9	725.2	183.8
ML2, ML3	V-shaped semi-floating	979.9	1406.0	669.3	113.1
	Modified V-shaped semi-floating	976.1	1340.7	756.7	92.4

The time domain responses of the two platforms in the last 1000 s out of 4000 s simulation time in Figure 9 show that the mooring performance of the modified V-shaped semi-floating is similar to that of the V-shaped semi-floating. It can be clearly seen that both the maximum mooring line forces of the modified V-shaped semi-floating are slightly lower than those of the V-shaped semi-floating, while the minimum mooring line force is higher than those of the V-shaped semi-floating. The standard deviation value of mooring line force in the modified V-shaped semi-floating is slightly smaller than that of the V-shaped semi-floating, and the average mooring line force is similar with V-shaped semi-floating. The statistical results reveal that the mooring performance of the modified V-shaped semi-floating is slightly better than that of the V-shaped semi-floating.

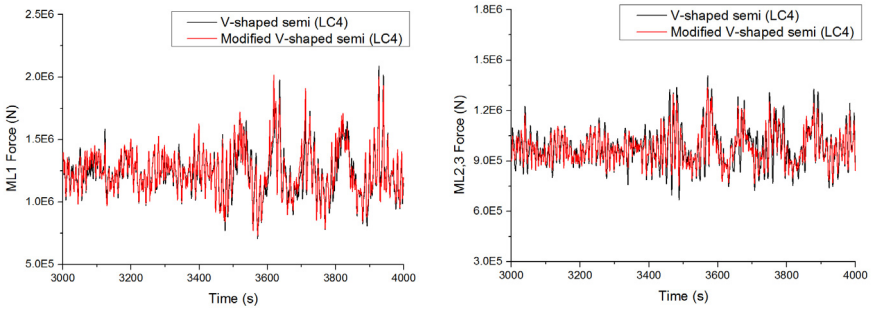

Figure 9. Mooring line forces under LC 4

In Figure 10, the power spectrum density of mooring line force in the extreme sea state (LC 4) are presented. It is clear in Figure 10 that the spectra of the mooring line force of the two platforms consist of two parts: (a) the low-frequency part, which is related to resonant responses of the platform and (b) the wave frequency part. More than one peak is observed in the low-frequency part (both surge and pitch resonant peaks are presenting for mooring line force spectrum).

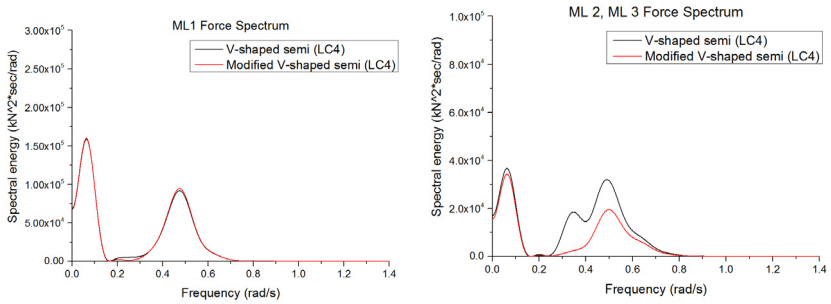

Figure 10. Mooring line force spectra under LC 4

4.3.4 Second order force effect. In Figure 11, the second-order force effect is investigated for both V-shaped semi-floating and modified V-shaped semi-floating. Second order response in heave motion is more significant than the first order response near heave natural frequency (0.25 rad/s). However, the amplitude is still smaller than the response obtained for the wave frequency. The heave motion of the modified V-shaped semi-floating at pitch frequency (0.31 rad/s) was suppressed compared with original V-shape semi-floating. A reduction in response is identified at the wave frequency for modified V-shaped semi-floating. For pitch motion, it shows that second order force makes a great contribution to the pitch motion near heave natural frequency compared to the contribution of the first order force, which makes it different from heave response. There is a large response reduction at pitch natural frequency for the modified V-shaped semi-float

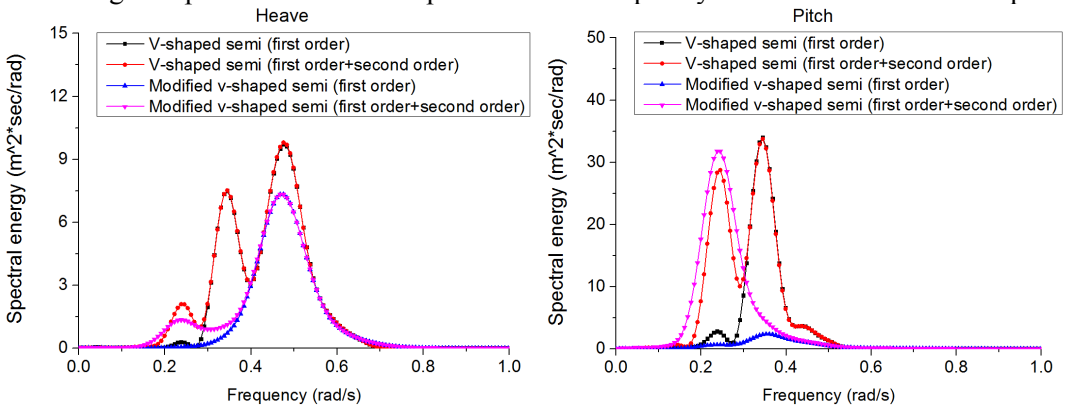

Figure 11. Comparison of motion spectra under LC4 with first order force and second order force

5 Conclusions

In this paper, the dynamic responses of motion and mooring line loads for the modified V-shaped semi and the V-shaped semi FOWTs under wave-wind induced loads are simulated. Based on the numerical results, we obtain the following conclusions:

(1) The modified V-shaped semi-floating shows better motion performance than the V-shaped semi-floating. It is found that the two platforms perform quite well during examined wind and wave load cases. The motion statistics are quite acceptable in consideration of the chosen significant wave height. The modified V-shaped semi-floating shows better performance than V-shaped semi-floating. For instance, compared with V-shaped semi-floating, the heave motion ranges of the modified V-shaped semi-floating are reduced by 20%, while the pitch motion ranges are reduced by 46%, under extreme combined wind-wave condition.

(2) The mooring performance of the modified V-shaped semi-floating is slightly better than the V-shaped semi-floating. The standard deviation values of the ML 2 and ML 3 forces are reduced by

18% under LC 4, which means less fatigue load to reduce the chance of breaks in the mooring line. It can also be concluded from Figure 8 that the spectrum of mooring line force is not only affected by surge motion but also by pitch motion.

(3) In the future, the short-term fatigue life of mooring lines should be considered because it is directly related to costs. The fully coupled analysis should also be conducted to consider the effect of wind turbulence and aerodynamic load.

Acknowledgements
The authors would like to gratefully acknowledge financial support from the National Natural Science Foundation of China (Grant No. 51709039, 51709040). This work is partially supported by the international collaboration and exchange program from the NSFC-RCUK/EPSRC (51761135011) and the Fundamental Research Funds for the Central University (DUT19GJ209).

References:

[1] Young E 2015. *Offshore wind in Europe: walking the tight rope to success*
[2] Heronemus W E 1972 *Proc. of Annual Conference and Exposition Marine Technology Society* (Washington)
[3] Liu Y, Li S, Yi Q, and Chen D 2016 *J. Renewable and Sustainable Energy Reviews* **60** 433-449
[4] Madslien J. "Floating challenge for offshore wind turbine". BBC News. Retrieved 14 September 2009.
[5] "Hywind Scotland, World's First Floating Wind Farm, Performing Better Than Expected | CleanTechnica". cleantechnica.com. Retrieved 7 March 2018.
[6] Bulder B H, Hees M T, Henderson A, Huijsmans, Pierik J, Snijders E and Wolf M 2002 *Public Report*
[7] Robertson A, Jonkman J, Masciola M, Song H, Goupee A, Coulling A and Luan C 2014 *NREL report*
[8] Roddier D, Cermelli C and Weinstein A 2009 *Proc. of the ASME 28th Int. Conf. on offshore Mechanics and Arctic Engineering* (Hawaii)
[9] Xu K, Gao Z and Moan T 2018 *15th Deep Sea Offshore Wind RD Conference* (Trondheim)
[10] Karimirad M and Michailides C 2015 *J. Energy Procedia* **80** 21-29
[11] Karimirad M and Michailides C 2015 *J. Renewable Energy* **83** 126-143
[12] Karimirad M and Michailides C 2016 *J. of Renewable and Sustainable Energy* **8** 89-144
[13] Michailides C and Karimirad M 2015 *J. of Recent Patents on Engineering* **9** 104-112
[14] Karimirad M and Michailides C 2018 *J. of Marine Science and Technology* 1-12.
[15] Robertson A and Jonkman J 2011 *NREL report*
[16] Aubault A, Cermelli C, Roddier D 2009 *Proc. of the ASME 28th Int. Conf. on offshore Mechanics and Arctic Engineering* (Hawaii)
[17] LandbØ T 2013 *OO Star Wind Floater A robust and flexible concept for floating wind*
[18] Lopez-Pavon C and Souto-Iglesias A 2015 J. *Renewable Energy* **81** 864-881.
[19] Jiang Y, Hu G, Jin G, Sun Z, Li J, Zong Z 2018 *Proc. of the Twenty-eighth Int. Ocean and Polar Engineering Conference* (Sapporao)